Bearing fault detection in brushless DC motors: a sensitivity study

Pavle Boškoski, Bojan Musizza, Janko Petrovčič, Đani Juričić

***Abstract*— Guaranteeing 100% fault free products is becoming an emerging standard in many branches of manufacturing. In this paper we examine the sensitivity of envelope analysis, spectral kurtosis and cyclostationary analysis methods. The objective was to determine the most suitable signal processing method for bearing fault detection in final quality assessment system for a production line of brushless DC motor. The method's sensitivity was evaluated on the most common bearing faults: inner race, outer race, roller bearing fault and lack of lubrication. Results indicated that cyclostationary analysis and spectral kurtosis have better sensitivity then than the envelope analysis.**

I. Introduction

Fault detection techniques based on vibration signals are one of the most commonly used approaches in the field of fault detection. This is mainly due to their non–invasive nature and their high reactivity to incipient faults.

Due to the fact that most mechanical faults occur in the rolling bearing, they have been in the focus of the fault detection research. The basic principles of the bearing fault detection were laid by McFadden [10]. The characteristic frequencies produced by a localized bearing faults were device by Tandon [16]. Variety of signal processing techniques have been used for bearing's fault detection. Envelope analysis as one of the most established methods has been extensively used [8], [14]. Equally large is the number of authors detecting the bearing faults using time–frequency approaches such as wavelet transform [12], [14]. With the development of the probabilistic bearing vibration model by Randall [13], the usage of different methods such as spectral kurtosis [15], [5] and cyclostationary analysis [9], [2] have been employed.

In this research we investigated the problem of incipient mechanical fault detection on a production line of blushless DC motors. Our results show that in cases of severe bearing inner and outer race faults, the commonly used envelope analysis is sufficient for the symptom generation task. However the cases of improper bearing lubrication or bearing damages due to inappropriate mounting have shown to be difficult to detect by simple spectral analysis of the signal's envelope. The main problem in these cases is that the extracted features resamble the fault–free case, so the faulty EC motor under investigation is indistinguishable.

For resolving this difficulty we have analyzed the vibration signals using two methods: spectral kurtosis (SK) and cyclostationary analysis. Both methods can be used for a detection of frequency bands where the impulses generated by the localized bearing faults are most distinguishable, thus simplifying the fault detection process..

In this work we have used a probabilistic bearing vibration model, which in short is presented in Section II. A brief overview of the theory behind the used signal processing algorithms is given in Section IV. The remaining sections of the paper cover the sensitivity analysis of each method.

All authors are with Jožef Stefan Institute, 1000 Ljubljana, Slovenia
pavle.boskoski@ijs.si

II. Model of bearing vibrations

Most frequently, bearing faults include surface damage of the inner or outer rings as well as the rolling bearing elements. When such a fault appears, the passing rolling element will generate an impact which will excite impulse response $s(t)$ of the observed system. These impacts will occur on every pass of a roller element over the localized fault, thus exiting periodic impulse responses $s(t - iT)$, where T is the time between consecutive impacts. However, due to random slip, as well as random speed fluctuations the occurrence of these impulses will not be strictly periodic, but some randomness should be introduced. Finally, the 'quasi-periodic impulse responses will now occur $s(t - iT - \tau_i)$, where τ_i is the random fluctuations of the occurrence of the i^{th} impact. Consequently, the final model for vibrations produced by a bearing with localized fault may be modeled as [13]

$$x(t) = \sum_i A_i s(t - iT - \tau_i) + n(t). \qquad (1)$$

where $x(t)$ is the vibration signal, A_i is the random impact amplitude. The addition part $n(t)$ represents the contribution of other vibration sources as well as the environmental influence, which all togeather is considered as noise.

III. Observed bearing faults

For the purpose of bearing fault detection we have analyzed the vibration signature of the observed motor for cases when the motor was running with damaged bearing. The conducted experiments covered 5 cases: fault–free motor, bearing inner race fault, bearing outer race fault, foreign debris fault and bearing without lubrication. The selected faults cover the set of most common bearing faults that can occur during motor's production process.

All test were done under same controlled rotational speed $f_{rot} = 38$Hz. During the tests none of the examined motors was loaded. Both motor bearings were FAG 6205. The characteristic bearing fault frequencies calculated for f_{rot} are shown in Table I.

TABLE I

CALCULATED BEARING FREQUENCIES FOR FAG 6205

Bearing fault	Frequency [Hz]
Ball passing frequency inner race (BPFI)	204.8Hz
Ball passing frequency outer race (BPFO)	135Hz
Fundamental train frequency (FTF)	15Hz
Ball spin frequency (BSF)	89Hz
Rolling element defect frequency	178Hz

IV. SIGNAL PROCESSING TECHNIQUES

A. Envelope analysis

The information about the type localized bearing fault can be extracted by monitoring the time between two consecutive impulses. Since the amplitude of these impacts can vary sometimes can be quite difficult the estimate exactly when does the impact occurs. The quasi-periodic occurrence of the impulses leads to an idea of analyzing the spectrum of the signal's envelope.

The spectrum of the envelope signal can be obtained on the basis of Hilbert transform, by calculating the spectrum of the analytical signal $x_a(t)$, obtained from the observed signal $x(t)$. The analytical signal $x_a(t)$ is a complex signal whose real part is the original signal $x(t)$, and the imaginary part is the Hilbert transform of the original signal $x(t)$

$$x_a(t) = x(t) + i\mathscr{H}[x(t)], \tag{2}$$

where $\mathscr{H}[x(t)]$ is the Hilbert transform of the signal $x(t)$

$$\mathscr{H}[x(t)] = \frac{1}{2\pi}\int_{-\infty}^{+\infty}\frac{x(t)}{t-\tau}\,d\tau. \tag{3}$$

The analytical signal has spectrum only in the positive frequency range.

The envelope of the original signal $x(t)$ can be obtained by calculating the amplitude of the analytical signal (2)

$$a(t) = \sqrt{x^2(t) + \mathscr{H}^2[x(t)]}. \tag{4}$$

1) Results from envelope analysis of the acquired signals: The acquired vibration signals, were initially lowpass filtered at 22 kHz, and then sampled at 60 kHz. The envelope analysis was applied without any additional signal conditioning.

Fault free The envelope spectrum of the fault–free motor (cf. Figure 1 first subplot), running under nominal speed f_{rot}, is dominated by two spectral components $10 \times f_{rot}$ and $20 \times f_{rot}$. The components are actually the first and third harmonic of the power supply pulse width modulation frequency $f_{pwm} = 5 \times f_{rot}$. The factor 5 is due to the 5 poles in the observed brushless DC (BLDC) motor.

Debris fault The case of debris fault yield almost continuous envelope spectrum, cf. the second sub-plot in Figure 1. Such spectrum is a result of high–energy random impulses produced each time when some of the debris obstructed any of the rotating roller elements.

Lack of lubrication fault The spectrum of lack of lubrication fault, third sub-plot in Figure 1, is very similar to the one of the fault free case. Although it was expected for the spectrum to contain some spectral component characteristic

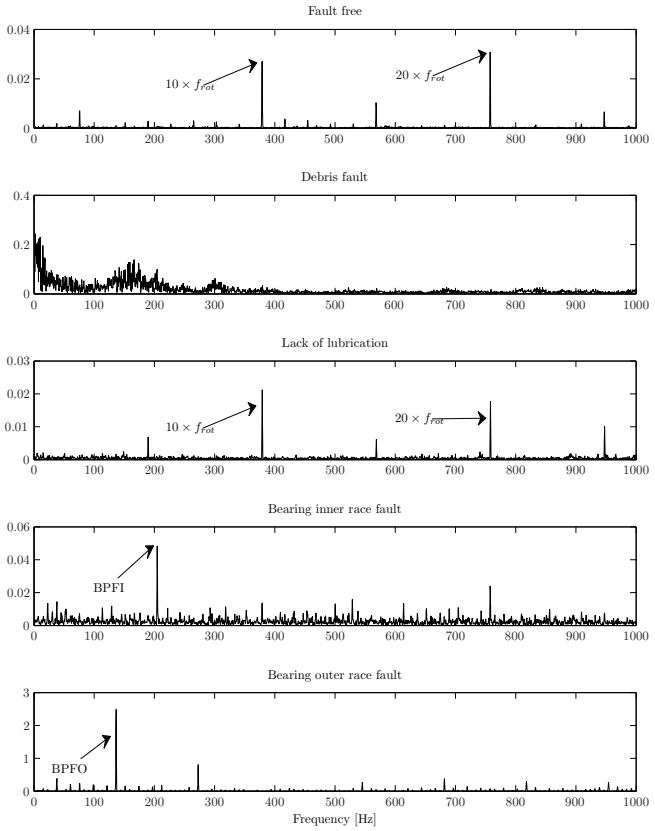

Fig. 1. Envelope spectra of the vibration signal

for the particular fault, the spectrum contains the same spectral components as the fault–free case. Even more, the amplitudes of the dominant spectral components are smaller then the corresponding one in the fault–free case, which might lead to a false conclusion that the motor runs better in this case than in the fault–free one.

Unlike the lack of lubrication faults, the bearing inner and outer race faults, shown in the last two sub-plots in Figure 1, are clearly distinguishable. Both are dominated by the characteristic frequencies for the particular bearing faults, BPFI and BPFO respectively.

From this simple analysis we can conclude that the envelope analysis is effective only in cases where the faults excite significantly powerful impulses, like bearing inner and outer race faults. Conversely, the pulses excited by the lack of lubrication fault have significantly smaller amplitudes and they are indistinguishable from the vibrations produced by other vibration sources. In order to resolve this issue, we had to analyze the vibration signals using different methods that are more effective in detecting impulses masked by noise.

B. Spectral kurtosis

The spectral kurtosis (SK) method was firstly introduced by [4]. It was used as a filter to recover randomly occurring signals severely corrupted by additive stationary noise. As with standard kurtosis, spectral kurtosis, takes high values for frequency bands where the vibration signal $x(t)$ defined with (1) is dominated by the corresponding impulses. On the

other hand it takes low values for frequency bands where the signal is dominated by the noise $n(t)$ [3]. If we rewrite the signal from (1) as

$$x(t) = y(t) + n(t), \tag{5}$$

where

$$y(t) = \sum_i A_i s(t - iT - \tau_i), \tag{6}$$

than the SK values for the signal $x(t)$ contaminated by additive noise $n(t)$ can be calculated as [3]

$$K_x(f) = \frac{K_y(f)}{[1 + \rho(f)]^2}, \tag{7}$$

where $K_y(f)$ is the spectral kurtosis of the signal $y(t)$, and $\rho(f)$ is the noise–to–signal ratio for that particular frequency f. The value for $K_y(f)$ can be obtained using the following relation

$$K_y(f) = \frac{S_{4y}(f) - 2S_{2y}^2(f)}{S_{2y}^2(f)}, \tag{8}$$

where $S_{2y}(f)$ and $S_{4y}(f)$ are the second and fourth spectral moments respectively. The maximum of (7), actually determines the frequency band where the signal–to–noise ratio in the observed signal is the biggest and in the same time the closest to the original, uncontaminated signal, $y(t)$.

The statistical definition of SK given by the (8) bears resemblance with the statistical definition of kurtosis. However the actual physical interpretation and its ability for detection of non-stationary transients in signals is not so obvious. One way to clarify this issue is to observe the definition (8) through its "instantaneous" spectrum i.e. the spectrum of the signal observed at particular moment t. Averaging all these spectra over time we obtain the well known Welch's estimate of the power spectral density (PSD), which is independent of time t. Observing the temporal displacement of a particular frequency f, compared to its average value computed by the PSD we obtain the value for SK at that observed frequency. For non–stationary processes these displacements will be more expressed then in the cases of stationary processes. Consequently, we can use the SK as a indicator for a frequency band where the signal's non–stationarities are most expressed.

This observation leads to the conclusion, that the spectral kurtosis method searches for the optimal bandpass filter that maximizes the kurtosis of the filtered signal. Since our goal is to detect the irregular impacts in the signals, by maximizing the spectral kurtosis we achieve this goal.

1) Results from spectral kurtosis analysis of the acquired signals: By applying the SK method we obtained frequency bands parameters for each fault where the observed bearing fault impulses are most expressed. The envelope spectra of the signals filteret in the propused frequency bands are shown in Figure 2. The frequency band parameters of each fault are presented in Table II.

Fault–free case The spectrum of the fault–free, as expected, is dominated by the spectral components at $10\times$ and $20 \times f_{rot}$.

TABLE II
BANDPASS FILTER PARAMETERS

Fault	Central Frequency f_c	Bandwidth B_w
Fault free	12.2kHz	1875Hz
Debris fault	10.1kHz	469.5Hz
Lack of lubrication	937.5Hz	1875Hz
Bearing inner race fault	5.3kHz	625Hz
Bearing outer race fault	312Hz	625Hz

Lack of lubrication Unlike the enevelope analysis of the unfiltered signal, the spectrum of the envelope of the singal filtered in the frequency band determined by the SK method shows significant differences from the fault–free case. The spectrum is dominated by the spectral component and FTF (fundamental train frequency). This component is not visible in the fault-free state because presence of lubrication damps the vibrations caused by the rolling bearing elements. This effectively removes or significantly attenuates the FTF spectral component. Since there is no lubricant to act as a damper, these vibrations are clearly visible in the envelope spectrum.

Apart from FTF component, lack of lubrication spectrum contains spectral components of bearing outer race fault. This is due to the fact that the BPFO is 9^{th} harmonic of FTF, i.e. $BPFO = Z \times FTF$, where Z is the number of rolling elements. The amplitude of this component is quite smaller then the corresponding one in the case of pure outer ring fault. Since the mentioned components are not present in the fault free case they can be used as an additional feature for detection of this fault.

Bearing inner and outer race fault The last two sub-plots are the bearing inner and outer race fault. The spectrum is dominated of the bearing inner race fault is dominated by the BPFI and its 2^{nd} harmonic. It should be noticed that the amplitudes of these components are several times larger then the amplitudes of the components in the fault-free case. Similarly, the spectrum of the outer race fault is dominated by the BPFO and its 2^{nd} harmonic. Since the severity of the outer race fault is quite bigger than the inner race fault, the amplitudes of the characteristic frequencies are even larger compared to the inner race fault.

The obtained results support the idea that by filtering the vibration signals in a specific frequency band one can obtain better sensitivity, especially for incipient faults, like in the case of lack of lubrication fault. For further confirmation of this idea we have analysed the same vibration signals using different approach based on cyclostationarity of the vibration signals produced by rotational machines.

C. Cyclostationary analysis

A random process $x(t)$ is said to be *Nth order cyclostationary* if its Nth order distribution function exhibits periodicity with period T [11]

$$\begin{aligned} &F(x_1, x_2, \cdots, x_n; t_1, t_2, \cdots, t_n) = \\ &= F(x_1, x_2, \cdots, x_n; t_1 + mT, t_2 + mT, \cdots, t_n + mT) \end{aligned} \tag{9}$$

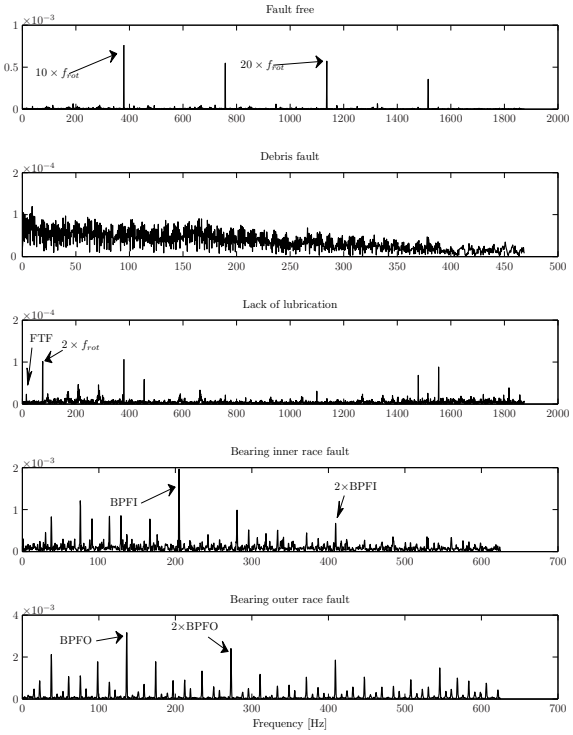

Fig. 2. Envelope spectra obtained in frequency bands which maximize the kurtosis

The process $x(t)$ is said to be wide–sense cyclostationary if its mean $E\{x(t)\}$ and its autocorrelation function $R_x(t,\tau)$ are periodic with period T [11]

$$\begin{aligned} E\{x(t)\} &= E\{x(t+T)\} \\ R_x(t,\tau) &= R_x(t+T,\tau) \end{aligned} \tag{10}$$

Due to the periodicity of the autocorrelation function and the assumption that Fourier series expansion is convergent [6], the autocorrelation function $R_x(t,\tau)$ can be expanded as

$$R_x(t,\tau) = \sum_{n=-\infty}^{+\infty} R_x^\alpha(\tau) e^{j2\pi\alpha t}, \tag{11}$$

where $\alpha = n/T$ also referred to as a *cyclic frequencies*, and $R_x^\alpha(\tau)$ are the Fourier coefficients of the autocorrelation function also referred to as *cyclic autocorrelation function*.

By analyzing the cyclic autocorrelation function it can be shown that the signal $x(t)$ and its frequency shifted version $x(t)e^{j2\pi\alpha t}$ are correlated [7]

$$R_x^\alpha(\tau) = E\left\{ x\left(t-\frac{\tau}{2}\right) x\left(t+\frac{\tau}{2}\right) e^{-j2\pi\alpha t} \right\}. \tag{12}$$

With a simple regrouping of the last equation we obtain

$$R_x^\alpha(\tau) = E\left\{ \underbrace{\left[x\left(t+\frac{\tau}{2}\right) e^{-j\pi\alpha(t+\tau/2)} \right]}_{u(t)} \underbrace{\left[x\left(t-\frac{\tau}{2}\right) e^{-j\pi\alpha(t-\tau/2)} \right]}_{v(t)} \right\}. \tag{13}$$

The multiplication with $e^{\pm j\pi\alpha t}$ actually causes a frequency shift of $\pm\alpha$ of the signal $x(t)$ in the frequency domain. This leads to a conclusion that the cyclic autocorrelation function of a random process $x(t)$ is cross–correlation of a frequency shifted versions $u(t)$ and $v(t)$ of the same signal $x(t)$. In should be noted that for $\alpha = 0$ the relation(13) reduces to a normal autocorrelation function. It can be concluded that a signal exhibits cyclostationarity at cyclic frequency α if $R_x^\alpha(\tau) \neq 0$.

In the same way that the power spectrum can be obtained by taking the Fourier Transform of the autocorrelation (the Wiener-Khinchin theorem), taking the Fourier Transform of the cyclic-autocorrelation with respect to the lag τ produces the cyclic spectrum or also called cyclic spectral density

$$S_x^\alpha(f) = \int_{-\infty}^{+\infty} R_x^\alpha(\tau) e^{-j2\pi f\tau} d\tau. \tag{14}$$

Similarly, for $\alpha = 0$ relation (14) reduces to the standard power spectrum. Equivalently, we can define a spectral autocoherence function based on a definition for coherence as:

$$\rho_x^\alpha(f) = \frac{S_x^\alpha(f)}{[S_x^\alpha(f+\alpha/2) S_x^\alpha(f-\alpha/2)]^{1/2}} \tag{15}$$

The function $|\rho_x^\alpha(f)|$ is bounded to the interval $[0,1]$, and it represents a time–averaged correlation coefficient for the process $x(t)$ at two frequencies $f \pm \alpha/2$. The values of autocoherence function that are close to 1 $\rho_x^\alpha(f)$ indicates whether the observed signal exhibits cyclostationarity at cyclic frequency α. Conversely, when $\rho_x^\alpha(f) \approx 0$ then the observed signal has no cyclostationaryties at that cyclic frequency

1) Results obtained by cyclostationary analysis: The plots of the cyclic correlation (15), shown in Figure 3, can be interpreted as following [1]:

1) The existence of a component at cyclic frequency α is connected to a fault signature, and
2) The values of a particular component read on f axis gives the signal-to-noise ratio of the fault for particular frequencies f.

Interpretation using rule 1): The spectral cyclic coherence (SCOH) for fault free case is shown in Figure 3(a). The dominant cyclic frequencies are $5\times, 10\times, 15\times, 20\times f_{rot}$. The components of the f_{rot} are visible between these mentioned lines. In particular the space between each dominant cyclic frequency is divided by four equally spaced components each spaced by f_{rot}.

Debris fault The randomness of the vibration signal acquired for the foreign debris fault is yet again confirmed by a nearly continuous cyclic spectral components on the α axis, as shown in Figure 3(b). The cyclic components due to the rotation are visible only in the frequency band above 10kHz. Below, on the other hand, there are no distinguishable cyclic spectral components.

Lack of lubrication fault The lack of lubrication state, shown in Figure 3(c), is very similar to the fault free case. The dominant cyclic frequencies are $10 \times f_{rot}$ and

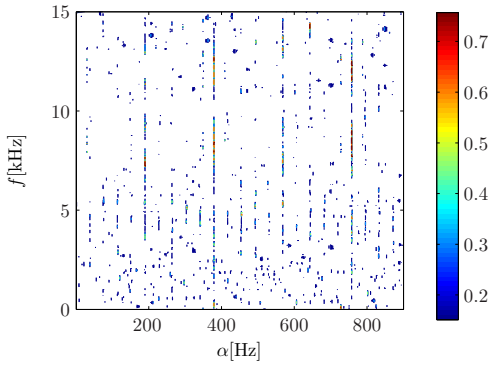

(a) Fault free

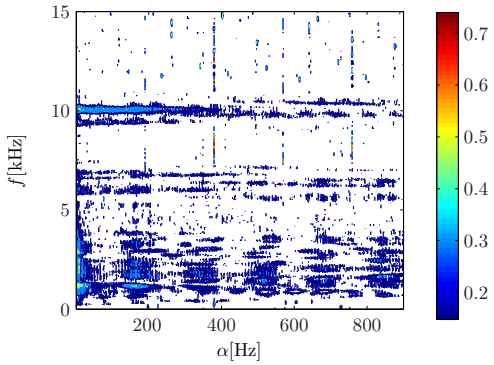

(b) Debris fault

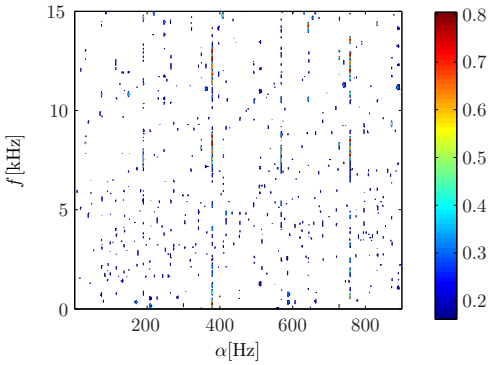

(c) Lack of lubrication

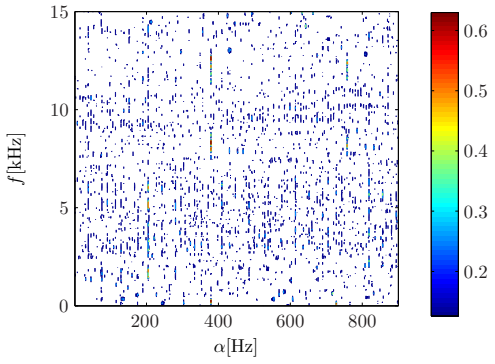

(d) Inner race fault

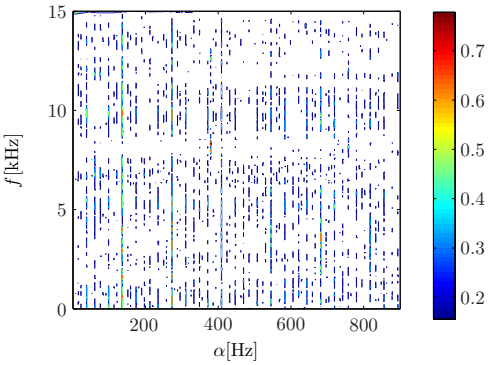

(e) Outer race fault

Fig. 3. Cyclic spectral coherence (SCOH) for vibration signal

its harmonics. The cyclic coherence for this case does not contain any additional cyclic spectral component that might point towards a specific fault.

Inner race fault Cyclic coherence for this fault is shown in Figure 3(d). We can detect a new cyclic component at 204Hz. This is a clear match with the BPFI frequency.

Outer race fault Similarly, outer race fault exhibits a strong cyclic component at 135Hz which is BPFO. This is shown in Figure 3(e).

Interpretation using rule 2): According to the Rule 2), the most appropriate frequency band lies with in the interval where the SCOH at the dominant cyclic frequency α has maximum value. Consequently, the first step would be a selection of the dominant cyclic frequency α for each fault and then examine the value of the SCOH on f-axis at that fixed cyclic frequency α.

The dominant cyclic frequencies for each fault are shown in Table III. The plots of SCOH for these selected frequencies are shown in Figure 4. By comparing the amplitudes of this cyclic component between lack of lubrication and fault–free state (cf. Figure 4(a)) we can determine the frequency band where the difference between these two cases is the biggest is in the interval [0-1.8kHz].

TABLE III

BANDPASS FILTER PARAMETERS OBTAINED BY CYCLOSTATIONARY ANALYSIS

Fault	Dominant cyclic frequency α
Lack of lubrication	$10 \times f_{rot}$
Bearing inner race fault	BPFI
Bearing outer race fault	BPFO

For the case of bearing inner race fault he plot is shown in Figure 4(b). The frequency interval where the SCOH has its maximum is in the frequency band between 4.5kHz and 5.5kHz. Similar observation can be made for the bearing outer race fault. By using the same approach as in the inner race fault the selected frequency band is between 0 and 1200Hz (Figure 4(c)).

According to this observation we have marked the most appropriate frequency bands for a particular fault in Figure 4. They are also listed in Table IV.

The most valuable result is the fact that the filter parameters obtained by the spectral kurtosis method (Table II) are almost identical to the ones obtained by the cyclostationary

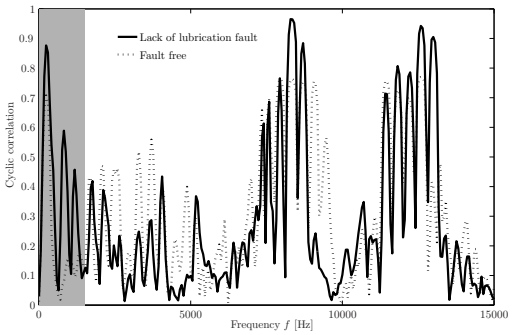

(a) Cyclic coherence of lack of lubrication and fault–free case for $\alpha = 387$Hz

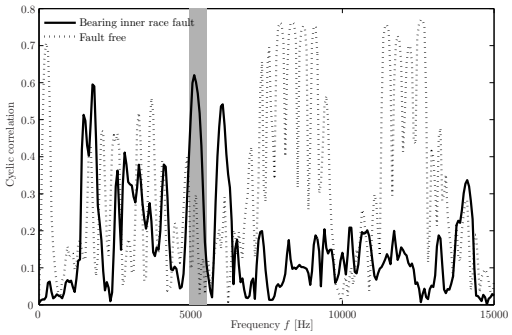

(b) Cyclic coherence of Bearing inner race fault and fault–free case for $\alpha = 204$Hz

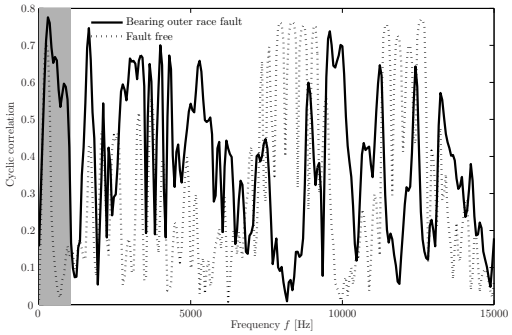

(c) Cyclic coherence of Bearing outer race fault and fault–free case for $\alpha = 135$Hz

Fig. 4. Frequency band selection based on the amplitude of SCOH at dominant cyclic frequency α

analysis (Table IV).

V. Conclusions

Spectral analysis of the unfiltered signals is not capable of detecting minute changes in the bearing state, like the lack of lubrication fault. One way of avoiding these difficulties is by filtering the original signals in specific frequency ranges that contain the best singal-to-noise ratio.

We have shown that the selection of the best band–pass filter parameters can be detected automaticly by using either spectral kurtosis or cyclostationary analysis. One problem with the cyclostationary analysis is the need to examine an interval of cyclic frequencies in order to find the most appropriate cyclic frequency α which is unique to the observed fault. However, as already pointed in [2], if we know the precise operating conditions, most importantly constant speed and load, we can calculate the spectral cyclic coherence only for a specific set of cyclic frequencies α and use them to detect and isolate faults.

Unlike the cyclostationary analysis, the spectral kurtosis is not very computationally demanding. Nevertheless both methods can be used for automatic fault detection. Even more the best frequency band is determined on–line and the implementation does not have to rely on excessive user's participation and expertise.

TABLE IV

Bandpass filter parameters obtained by cyclostationary analysis

Fault	Central Frequency f_c	Bandwidth B_w
Lack of lubrication	900Hz	1800Hz
Bearing inner race fault	5kHz	1kHz
Bearing outer race fault	600Hz	1.2kHz

References

[1] J. Antoni. Cyclic spectral analysis in practice. *Mechanical Systems and Signal Processing*, 21:597 – 630, 2007.

[2] J. Antoni. Cyclic spectral analysis of rolling-element bearing signals: Facts and fictions. *Journal of Sound and Vibration*, 304:497 – 529, 2007.

[3] J. Antoni and R.B. Randall. The spectral kurtosis: a useful tool for characterising non-stationary signals. *Mechanical Systems and Signal Processing*, 20:282–307, 2006.

[4] R. Dwyer. Detection of non-gaussian signals by frequency domain kurtosis estimation. *Acoustics, Speech, and Signal Processing, IEEE International Conference on ICASSP*, 8:607–610, 1983.

[5] H. Endo and R.B. Randall. Enhancement of autoregressive model based gear tooth fault detection technique by the use of minimum entropy deconvolution filter. *Mechanical Systems and Signal Processing*, 21:906–919, 2007.

[6] W. A. Gardner, A. Napolitano, and L. Paura. Cyclostationarity: Half a century of research. *Signal Processing*, 86:639 – 697, 2006.

[7] William A. Gardner. Exploitation of spectral redundancy in cyclostationary signals. *IEEE Signal Processing Magazine*, 8:14–36, 1991.

[8] D. Ho and R. B. Randall. Optimisation of bearing diagnostic techniques using simulated and actual bearing fault signals. *Mechanical Systems and Signal Processing*, 14:763–788, 2000.

[9] A. C. McCormick and A. K. Nandi. Cyclostationarity in rotating machine vibrations. *Mechanical Systems and Signal Processing*, 12:225 – 242, 1998.

[10] P.D. McFadden and J.D. Smith. Vibration monitoring of rolling element bearings by the high-frequency resonance technique - a review. *Tribology International*, 17:3–10, 1984.

[11] Athanasios Papoulis. *Probability, Random Variables, and Stochastic Processes*. McGraw-Hill, 1991.

[12] Z. Peng and F. Chu. Application of the wavelet transform in machine condition monitoring and fault diagnostics: a review with bibliography. *Mechanical Systems and Signal Processing*, 18:199–211, 2004.

[13] R. B. Randall, J. Antoni, and S. Chobsaard. The relationship between spectral correlation and envelope analysis in the diagnostics of bearing faults and other cyclostationary machine signals. *Mechanical Systems and Signal Processing*, 15:945 – 962, 2001.

[14] R. Rubini and U. Meneghetti. Application of the envelope and wavelet transform and analyses for the diagnosis of incipient faults in ball bearings. *Mechanical Systems and Signal Processing*, 15:287–302, 2001.

[15] N. Sawalhi, R.B. Randall, and H. Endo. The enhancement of fault detection and diagnosis in rolling element bearings using minimum entropy deconvolution combined with spectral kurtosis. *Mechanical Systems and Signal Processing*, 21:2616–2633, 2007.

[16] N. Tandon and A. Choudhury. A review of vibration and acoustic measurement methods for the detection of defects in rolling element bearings. *Tribology International*, 32:469–480, 1999.